Limitations of accuracy in PIV due to individual variations of particle image intensities

H Nobach and E Bodenschatz

Abstract

The effect of individual tracer particle intensity variations in consecutive images on the accuracy of the displacement estimates in particle image velocimetry is investigated. The achievable accuracy of PIV measurements is shown to be limited by this effect to approximately 0.1 pixels.

1 Introduction

Particle image velocimetry (PIV) has become the prime choice for processing image-based flow measurements in fluid dynamics experiments. The basic algorithm of digital PIV processing [1, 2, 3, 4] utilizes the cross-correlation of image sub-spaces for local displacement estimation from two consecutively acquired images of a tracer-particle-laden flow.

Using appropriate sub-pixel interpolation of the correlation planes, the achievable accuracy of the measurement of the particle displacement can be significantly improved over the nominal resolution of the optical sensor. Widely used in PIV are the peak centroid (center-of-mass) method [5, 6] and the Gaussian interpolation [2]. The remaining systematic error of the displacement estimate is periodic with respect to the discrete resolution of the sensor, yielding the "pixel locking" or "peak locking" [7, 8, 9, 10, 11] and limits the achievable accuracy. The pixel or peak locking effect is not investigated in this study, even if it is evident, However, the Gaussian interpolation of the correlation function [2], which also has been used here, performs well even for diffraction-limited intensity profiles of the particle images with intensity integration over uniformly sensitive sensor areas [12]. Advanced methods to further reduce this influence can be found e. g. in [13, 14].

The basic displacement estimator between sub-spaces (interrogation areas) of the two consecutive images utilizes the peak position of their cross-correlation obtained by means of the fast Fourier transform (FFT). If the real displacement of the particle pattern is small compared to the size of the interrogation areas, systematic errors due to the periodic boundaries are minor. A more important error is given by the fact that the interrogation areas have sharp edges. Particles lying on this edge are truncated and the center of the intensity distribution deviates from the position of maximum intensity. This affects the peak position in the correlation function and, therefore, limits the achievable accuracy of the displacement estimation [15].

A straight forward method to decrease the influence of truncated particle images is the application of a windowing function, which becomes zero at the interrogation area boundaries [16, 17, 18]. However, even if the influence of the truncated particle images at the edges of the interrogation areas can be reduced with this technique, a new error is introduced, since the shape of the particle images becomes asymmetric and the center of the intensity distribution moves towards the origin of the interrogation areas [19].

An alternative is the direct correlation with a normalization. This can be done either asymmetrically, with a small interrogation area from the first image correlated with a larger area in the second image [9, 20, 21, 22] or symmetrically with two interrogation areas of the same size [12]. To reduce remaining errors due to asymmetries of the correlation coefficient function, a third method [15], also called "symmetric" utilizes the displacements estimates from the first, asymmetric direct correlation and a second direct correlation with a small interrogation area from the second image correlated with a larger area in the first image. Since the two correlations are, nonetheless, asymmetric and only the direction of correlation changes, the term "asymmetric, bi-directional" is used in this study instead.

A further improvement can be achieved by iteratively applying a shift and deformation of the interrogation areas [23, 24, 25]. This technique iteratively optimize the estimated velocity field towards vanishing displacements between image sub-spaces, which are shifted and deformed accordingly to the assumed velocity field. Because of the vanishing displacement, the results are almost independent of the utilized correlation plane sub-pixel interpolation scheme (correlation peak centered around zero) and of particle image truncations at the edges of the interrogation area (similar patterns in both interrogation areas are correlated). Nonetheless, the shifted and deformed image sub-spaces are obtained by re-sampling the original images at appropriate sub-pixel position. Thus, an appropriate image sub-pixel interpolation is required.

This holds true also for image deformation methods [26, 27]. Here the entire images are deformed accordingly to the assumed velocity field before the sub-devision into interrogation areas. The deformation's degree of freedom is related to the grid of velocity estimates, independent of the interrogation area size. With a high overlap of neighboring interrogation areas in combination with an iterative correction of residual displacements of the estimated velocity the spatial resolution is governed by the grid spacing without loosing the robustness of the large interrogation areas. Therefore, this method is gained to improve the achievable resolution of the PIV processing.

Unfortunately, with the original image deformation technique the iterations tend to become unstable with exponentially increasing deviations [16, 28]. The reason for these instabilities is the top-hat profile of the interrogation windows (top-hat windowing function to crop the interrogation area from the image), which yields negative values of the frequency response function in certain ranges of spatial frequencies. Due to the wrong sign of the displacement estimate, the displacement between the re-sampled images is increased instead of decreased and the velocity pre-estimate is even worse for the next iteration.

Of course, by applying a low-pass filter, which removes all components of the estimated velocity field at those frequency ranges, the instability can be removed. However, the characteristics of this filter must be adapted to the size of the interrogation window. This filter inturn limits the spatial resolution, which defeats the intention for improval. A superior solution is the application of appropriate windowing functions to the interrogation areas, which have frequency responses with only positive values [16]. This avoids the instability of the iterative optimization, while the resolution is not bounded by a low-pass filter. Because the frequency response of the velocity estimation procedure is positive for all frequencies, the distance between the estimated velocity and the correct velocity decreases with each iteration step and finally vanishes.

Since the accuracy of the velocity estimates by means of the interrogation area shift and deformation or image deformation directly depends on the quality of the image interpolation, the simple, but widely used, bi-linear interpolation yields poor results. Higher-order interpolation schemes have been shown to be advantageous [8, 13, 14, 29]. In particular, bi-cubic splines and the Whittaker interpolation [30, 31] (also known as sinc or cardinal interpolation) have found wide acceptance. In studies based on synthetic images an accuracy of the order of 0.01 pixel has been reported [24]. Recently, a Gaussian low-pass filter for image interpolation and re-sampling was introduced [32] to further improve the accuracy by reducing the system-inherent under-sampling of the particle images. In contrast, the application to real images from experiments shows less optimistic results, where the usually observed limit is of about 0.1 pixel. Only under special conditions, like in two-dimensional flows with carefully aligned light sheets, a better accuracy has been achieved [33].

A possible reason for the different achievable accuracy in simulations and experiments may be the fact that in experiments, particles usually change their position within the light sheet (figure **??**a). Therefore, the particles are illuminated differently in the two consecutive exposures. Additionally, the different illumination is individually different for each particle due to their different starting positions perpendicular to the light sheet plane, even if there is no gradient of the out-of-plane velocity component. The result is an individual variation of particle intensities.

Simulations often assume individual intensities for each particle, but identical intensities in the two exposures, as it can be realized in experiments only in two-dimensional flows with light sheets exactly aligned parallel to the flow field (figure 1b). On the other hand, individual intensity variations can be easily seen in images from a variety of PIV applications, where some particles become brighter between the two exposures, whereas other particles, even close by, become darker (figure 2).

Note that the case with individual variations of particle image intensities is different from

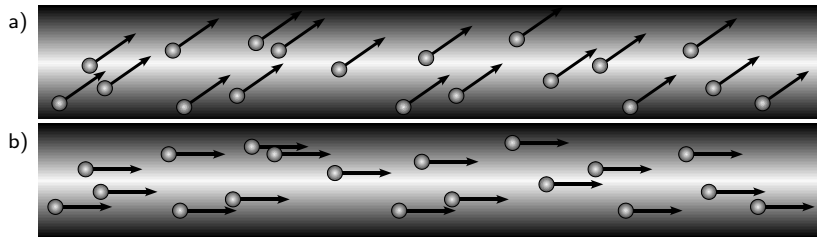

Figure 1: Particles moving in a light sheet with an intensity profile: a) with an out-of-plane component (all components may have gradients) and b) a two-dimensional flow aligned with the light sheet plane (only in-plane components may have gradients, out-of plane component must be zero)

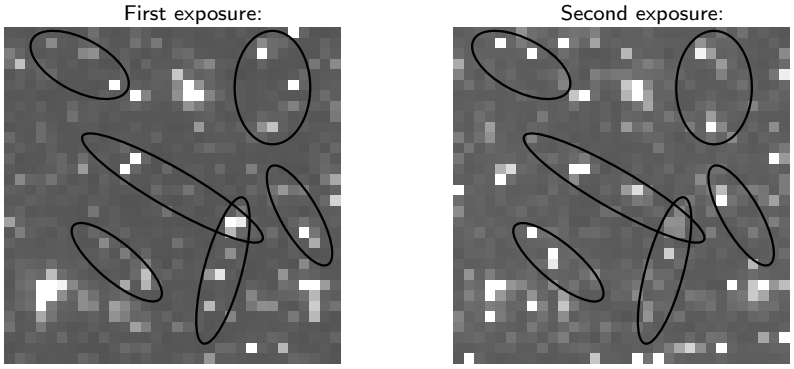

Figure 2: Example for individual particle intensity variations (detail of public PIV images from the PIV challenge 2003, case A, axisymmetric turbulent jet in stagnant surrounding, images A001a and A001b, marked regions with examples of individual particle intensity variations)

the loss-of-pairs and from the degradation of the correlation peak due to the out-of-plane motion [3, 34, 35, 36], large scale illumination variations [21] or intensity variations only due to the different particle locations within the light sheet without relative changes between the exposures [36]. While the loss-of-pairs increases the sensitivity to noise and the probability of outliers, the here discussed effect occurs additionally.

The present paper introduces the effect of the individually varied particle image intensity on the achievable accuracy of the above mentioned PIV processing techniques. Based on computer simulations, it is shown that the individually varied particle image intensity limits the achievable accuracy of the PIV processing to about 0.1 pixel even under otherwise ideal conditions.

2 Effect of varying intensities

In PIV the displacement of particle patterns between consecutive images is obtained from the peak position in the two-dimensional cross-correlation plane of the two images. Assuming (i) a certain number of imaged particles in the interrogation area, each with different intensity, but with the same relative intensity in the two consecutive images and (ii) no truncation at the edges of the interrogation areas, the correlation peak is at the correct position, even if the particle images overlap and if the intensity of one entire image is scaled by a constant factor. For demonstration, in Fig. 3 two signals, each consisting of two well separated peaks with Gaussian intensity profiles are correlated. The peaks are at identical positions in the two signals (no displacement between the signals). The correct position of the correlation maximum at zero displacement can be seen clearly even for overlapping intensity profiles and also with a constant scaling of one signal (Fig. 3b).

This holds true also for the correlation of Gaussian intensity profiles with different amplitudes[1], as long as the intensity profiles do not overlap in the individual signals (Fig. 4a). With

[1]Such variations of the intensity are typical for misaligned light sheets or particles moving out-of-plane, located at different intensity slopes of the light sheet profile

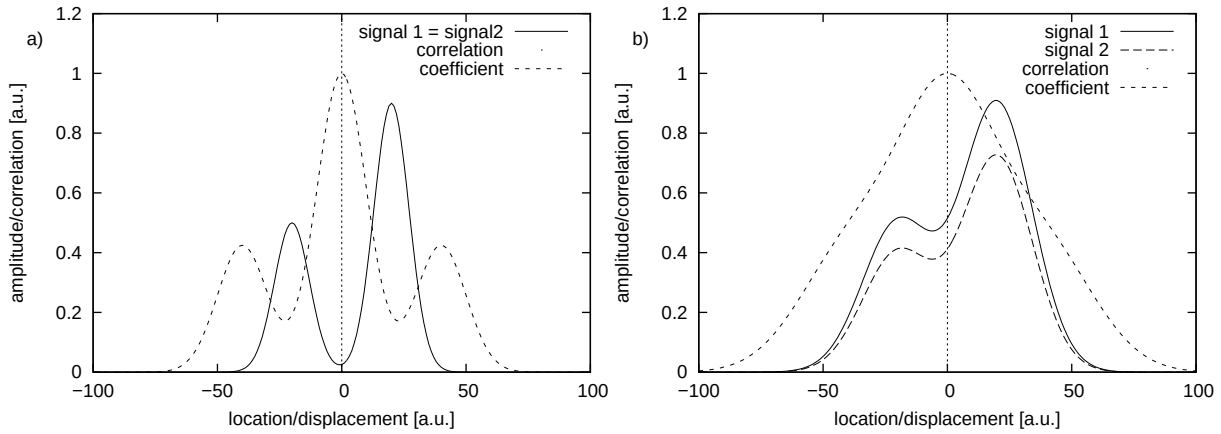

Figure 3: Intensity and cross-correlation function of two signals, each consisting of two peaks with Gaussian intensity profiles: a) same intensity of the profiles in the two signals with well separated peaks and b) one signal scaled and with overlapping peaks

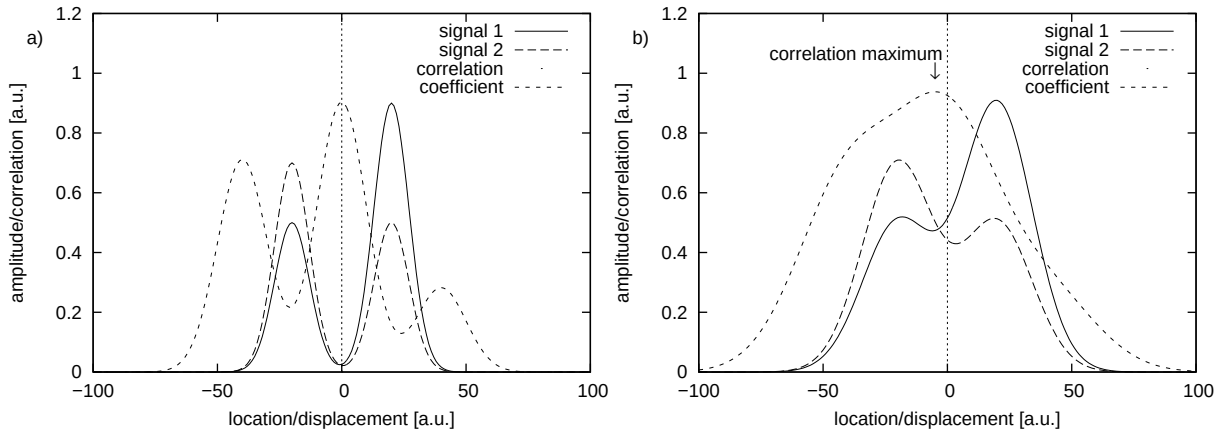

Figure 4: Intensity and cross-correlation function of two signals, each consisting of two peaks with Gaussian intensity profiles: a) varying relative intensity of well separated peaks and b) varying relative intensity of overlapping peaks yielding a correlation peak with a shifted maximum location

overlapping intensity profiles of varying amplitude (Fig. 4b), the maximum position of the correlation peak is clearly shifted, yielding a biased displacement estimate depending on the amplitudes of the intensity profiles, widths and overlap.

The consequence for PIV image processing is an additional error of displacement estimates, if the intensities of particle images vary between the consecutive PIV images, while the particle images overlap. This error is especially large in densely seeded flows or de-focussed images (where the particle images tend to overlap) and in the case of misaligned light sheets or flows with an out-of-plane motion of the particles (where the illumination of individual particles changes between the two light pulses).

3 Image generation

To consider the diffraction-limited imaging of small particles, the simulated particle images are represented by Airy functions integrated over the sensitive sensor areas (pixels). The pixels are assumed to be square with uniform sensitivity over the whole detector area. The simulated particles are uniformly distributed over the observation area. Except for the iterative image deformation, where a two-dimensional sinusoidal displacement field is simulated, the displacement of the particles between the two exposures is randomly chosen between -1 and $+1$ pixels, but constant for all particles, simulating a homogeneous velocity field. The Airy functions of the

particles are linearly superimposed. The maximum intensities of the consecutive particle images are calculated for each simulated particle independently from a double random process as the product of the particle visibility and the individual illumination. The visibility is a uniformly distributed random value between zero and unity. It is chosen individually for each simulated particle but the same for the two exposures. The illumination is given by the position of the simulated particle in the light sheet. The light sheet is assumed to have a Gaussian profile and the position of the particles is uniformly distributed within the light sheet. Depending on the simulated out-of-plane displacement of the particles, the position within the light sheet changes between the consecutive exposures yielding individual particle image intensity variations. All simulations have been done with and without photon and quantization noise. A number of 1000 photons and an 8 bit quantization have been assumed for the maximum particle image intensity. No background gray value have been added in this demonstration.

4 Image processing

4.1 One-Step Estimators

The basic displacement estimator between sub-spaces (interrogation areas) of the two consecutive images utilizes the peak position of their cross-correlation obtained by means of the fast Fourier transform (FFT). The sub-pixel location of the maximum is obtained by fitting a Gaussian function to the maximum of the correlation and its two direct neighbors, independently in x and y direction. To decrease the influence of truncated particle images, the interrogation areas can be weighted by applying a windowing function, which becomes zero at the boundaries. For comparison, a polynomial window function as in [16], a cosine to the 20^{th} window as in [18] and a Gaussian window as in [17] have been used.

Alternatively, direct correlation with a normalization is used. For comparison, the asymmetrical [9, 20, 21, 22], the asymmetrical, bi-directional [15] and the symmetrical [12] methods are realized.

4.2 Iterative Estimators

PIV algorithms with iterative shift and deformation of the interrogation areas [23, 24, 25] make use of a sub-pixel re-sampling of the consecutive images based on pre-estimates of the velocity field.

The first iteration is similar to the basic FFT displacement estimator. In the next and all following iteration steps, the two consecutive images are interpolated and re-sampled at positions shifted symmetrically by plus/minus half the pre-estimated displacement. Ideally, the two re-sampled images are identical and no displacement can be found between them. Remaining displacements can be used to iteratively correct the displacement pre-estimate. This iterative correction loop asymptotically approaches a vanishing displacement between the two re-sampled interrogation areas. The remaining deviation to the real displacement depends on the interpolation quality. The simple and widely used bi-linear interpolation has been used here for reference only, because of its insufficient results. The bi-cubic spline interpolation, the Whittaker interpolation [30, 31] and the Gaussian low-pass image interpolation [32] have been implemented based on a 11×11 pixel image sub-space.

To keep the investigations simple and to isolate the influence of variations of particle image intensities, velocity gradients have not been considered and window deformation has not been implemented for the interrogation area shift methods. The conclusions are equally applicable to the case of velocity fields with gradients. In that case, however, other well known effects, like limited spatial resolution or dynamic range issues, may additionally influence the results.

For the image deformation, the displacement for each individual pixel is calculated from the estimated velocity grid by bi-linear interpolation. According to the found displacement of a given pixel, the re-sampling from the original images is done by a symmetrical shift, similar to the interrogation area shift and deformation. To isolate the influence of the individual particle intensity variations from other errors, like image interpolation errors, the re-sampling of the images is done by re-calculating the image at the new sampling positions. This can be done only in simulations, since the particle positions are known.

5 Results

To show the effect of the individual particle intensity variation, several relations have been investigated. Especially, the influence on test cases is shown, which usually are used to demonstrate the superiority of advanced processing algorithms. This study shows, how the individual particle intensity variation changes these results. As a figure of merit the estimation error (difference between the estimated displacement and the true displacement of the particles between the two simulated exposures) is used from a series of individual simulation and estimation realizations. From the series of individual errors an averaged RMS error is derived and shown in the diagrams, regardless of the specific error source (systematic or random errors). Especially, outliers may lead to large deviations compared to the usual estimation uncertainties. If outliers occur in the test sequence, they can be identified as very large RMS deviation values in the following diagrams.

5.1 On-step and interrogation area shift methods

In the first test case the results of the above given algorithms are shown as a function of the particle image diameter. The diameter is defined by the first zero value of the Airy function. The particle number concentration is 20 in an interrogation area size of 32×32 pixel squared. In Fig. 5 the results are shown without an out-of-plane component of the simulated particle displacement and without noise. For small particle image diameters, all algorithms have problems due to the system-inherent under-sampling of the particle images leading to large RMS deviations for particle image diameters of 1 pixel. For increasing particle images, the under-sampling problem decreases and the RMS value decreases with an increasing particle image diameter. For particle image diameters above 3 pixels the influence of the interrogation areas border becomes evident and the RMS deviation value of the FFT algorithm without interrogation area windowing accordingly increases with the particle image diameter. All other algorithms (interrogation area windowing, direct correlation with normalization and interrogation area shift and deformation) successfully suppress this effect. The RMS values continue to decrease with an increasing particle image diameter. Above a particle image diameter of 3.5 pixels the one-step estimation procedures run into a limitation of the accuracy. The reason is the disagreement of the correlation peak interpolation function, which here is a Gaussian, and the true correlation peak shape, which is the cross-correlation of two spatially discrete functions gained from piece-wise integrated Airy functions. Here, the iterative interrogation area shift and deformation techniques are superior, because the iteration procedure asymptotically converges towards a symmetric correlation peak with a centered maximum, so that the final result is independent of the actual correlation peak interpolation method. Furthermore, the two interrogation areas, re-sampled from the interpolated images ideally are identical and have the same particle images truncated at the edges. Therefore, the particle truncation has no influence on the results.

The comparison between the FFT methods with different windowing function applied shows similar results. Also the direct correlation methods with different normalization shows similar results, while the direct correlation with normalization in general performs better than the FFT methods. Furthermore, the iterative interrogation area shift and deformation is even better, strongly depending on the quality of the image interpolation. Therefore, the simple bi-linear interpolation yields poor results, while both, the Whittaker and the bi-cubic spline interpolations are superior. The Gaussian low-pass interpolation yields the best results, because it reduces the influence of the under-sampling significantly due to the broadening of the particle images, while, on the other hand, the higher probability of particle image truncations at the interrogation area borders has no influence.

The simulation has been repeated with noise added to the images (Fig. 6). The comparison of the diagrams with the diagrams in Fig. 5 shows no significant influence of the noise to the methods ranking. Only the Gaussian low-pass interpolation shows the effect of the noise: a limitation of the achievable accuracy of about 0.001 pixel, which is not reached by any other processing method.

This image changes significantly, if the simulated particle displacement has an out-of plane component. In Fig. 7 the effect of an out-of plane displacement of $1/4$ of the light sheet width can be seen. All methods are strongly limited by this influence. The FFT methods and the direct correlation with normalization have comparable results and reach an accuracy of about 0.1 pixel. The probability of overlapping particle images increases with the particle image size and above 3 pixels diameter the influence of the individual particle image intensity variations dominates

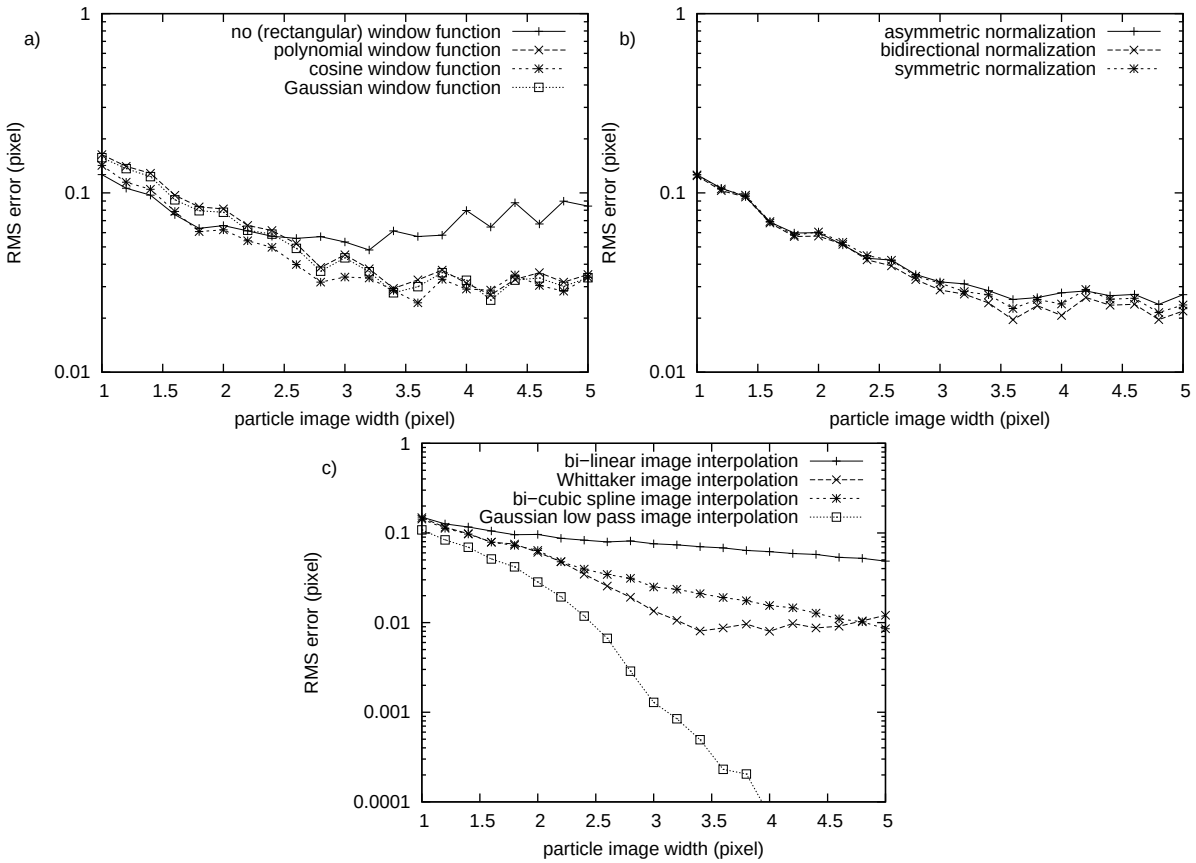

Figure 5: RMS deviation of the displacement estimate using a) the FFT with a window function b) the direct correlation with a normalization and c) the iterative interrogation area deformation with image interpolation as a function of the particle image diameter with only in-plane-motion

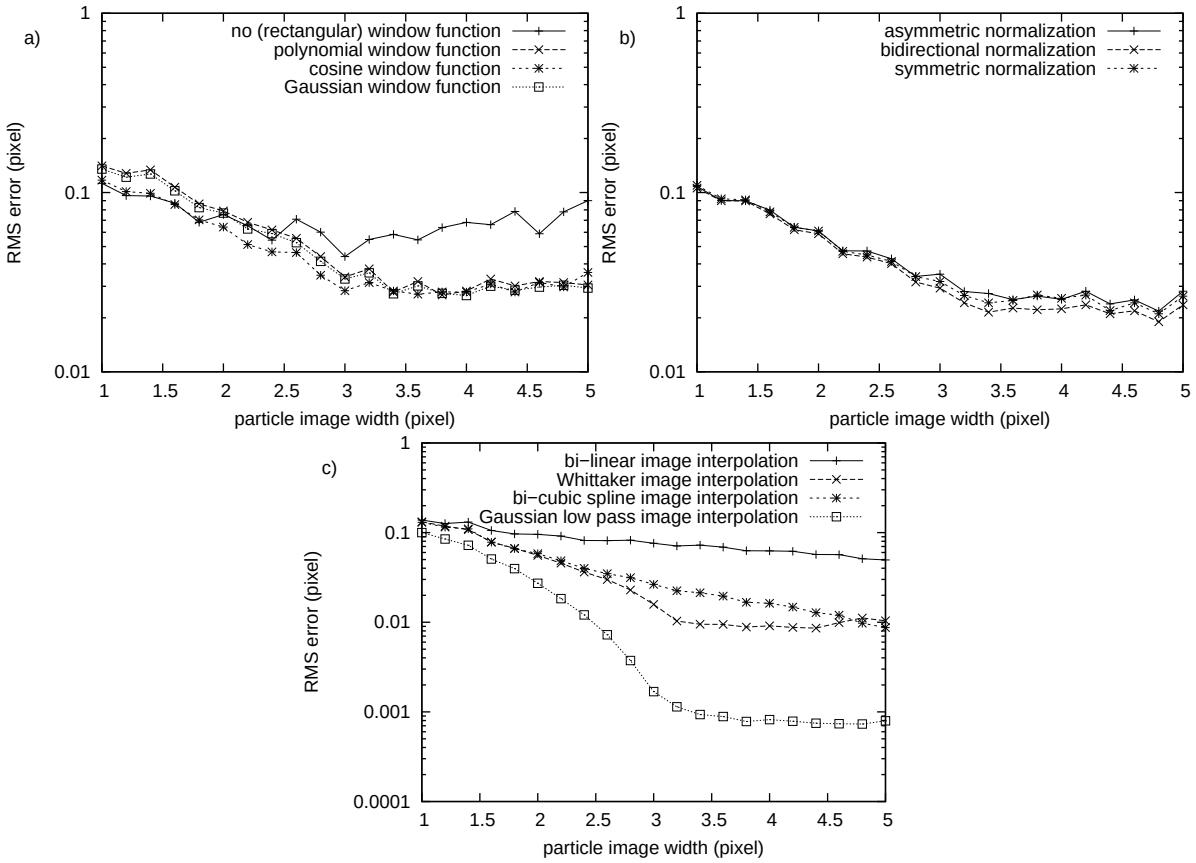

Figure 6: RMS deviation of the displacement estimate using a) the FFT with a window function b) the direct correlation with a normalization and c) the iterative interrogation area deformation with image interpolation as a function of the particle image diameter with only in-plane-motion and with noise

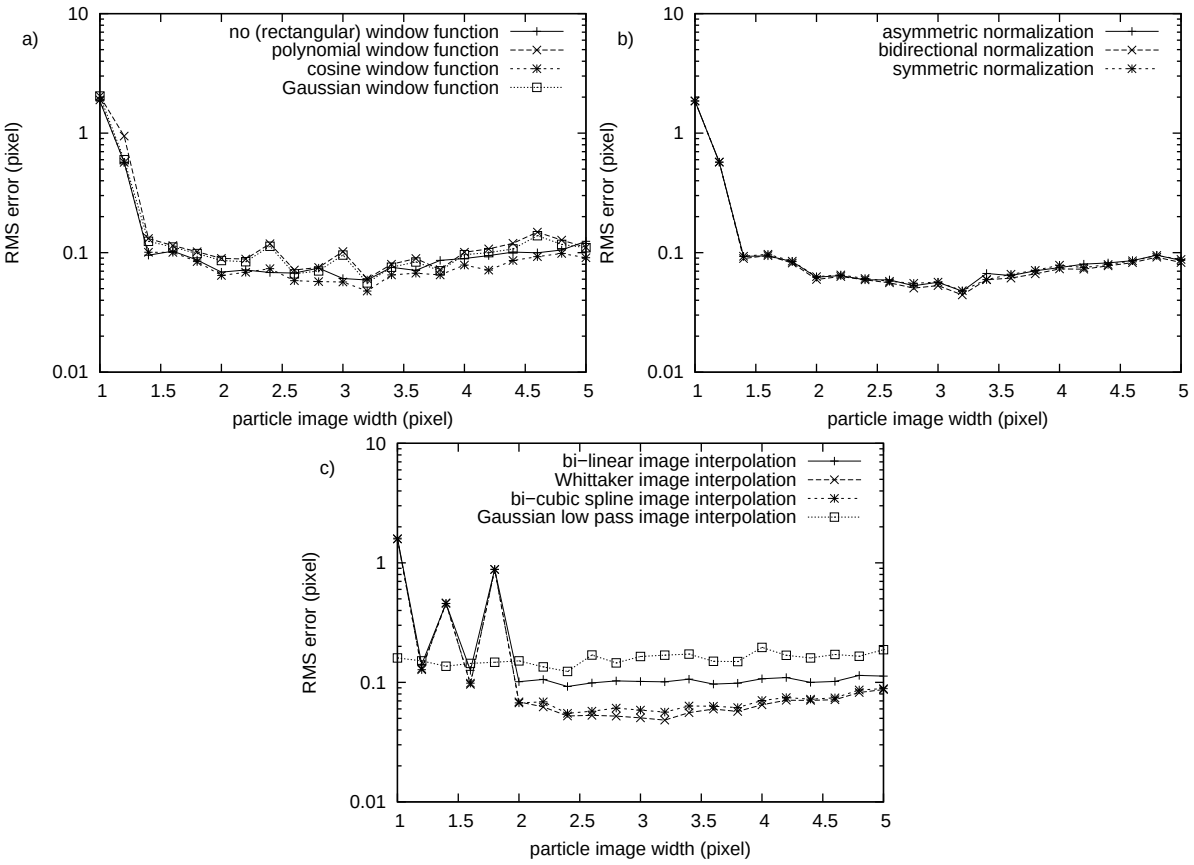

Figure 7: RMS deviation of the displacement estimate using a) the FFT with a window function b) the direct correlation with a normalization and c) the iterative interrogation area deformation with image interpolation as a function of the particle image diameter with out-of-plain motion (1/4 of the light sheet width)

the particle image under-sampling and the RMS deviation increases with the diameter of the particle images.

The methods with iterative interrogation area shift and deformation perform slightly better, where the Whittaker and the bi-cubic spline interpolations still yield better results than the bi-linear image interpolation. The largest effect can be seen on the Gaussian low-pass interpolation. Due to the broadening of the particle images after interpolation, the effect of the individual particle image intensity variations is dominating even for small original particle images and the results are even worse than for the bi-linear interpolation.

To show how important the out-of-plane displacement is, the simulation has been done also with a constant particle image diameter of 3 pixels with varying ont-of-plane displacements (Fig. 8). In principle, all algorithms show the same behavior: For small out-of-plane displacements the RMS value increases with the out-of-plane displacement until outliers occur at an out-of-plane displacement of about 35 % of the light sheet width. For larger out-of-plane displacements the estimation becomes unreliable. The ranking of the algorithms is similar as before. Only the iterative interrogation area shift and deformation with the Gaussian low-pass image interpolation shows an excellently small RMS value without the out-of-plane displacement, which rapidly increases with the increasing out-of-plane displacement and becomes worse than the other image interpolation methods.

To investigate the influence of the particle number concentration the simulation has been done also with different particle number concentrations at a constant interrogation area size of 32×32 pixel squared and a constant particle image diameter of 3 pixels and, exemplarily, an out-of-plane displacement of 1/4 of the light sheet width (Fig. 9). For a too small particle number concentration, the estimate is unreliable and yields outliers. For a particle number concentration larger than 0.01 per pixel squared the RMS value drops down and stays at a almost fixed level. Here, the increased content of available information due to the increased number of particle

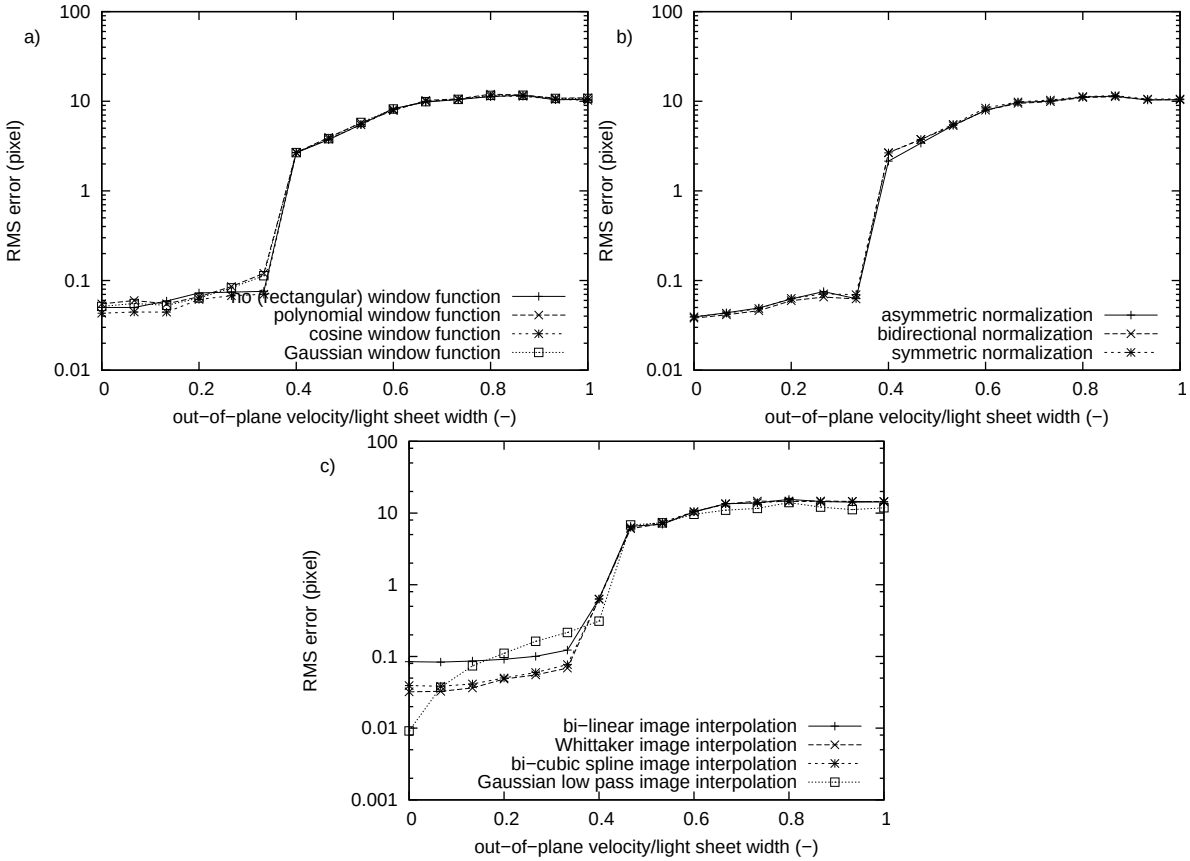

Figure 8: RMS deviation of the displacement estimate using a) the FFT with a window function b) the direct correlation with a normalization and c) the iterative interrogation area deformation with image interpolation as a function of the out-of-plane displacement component

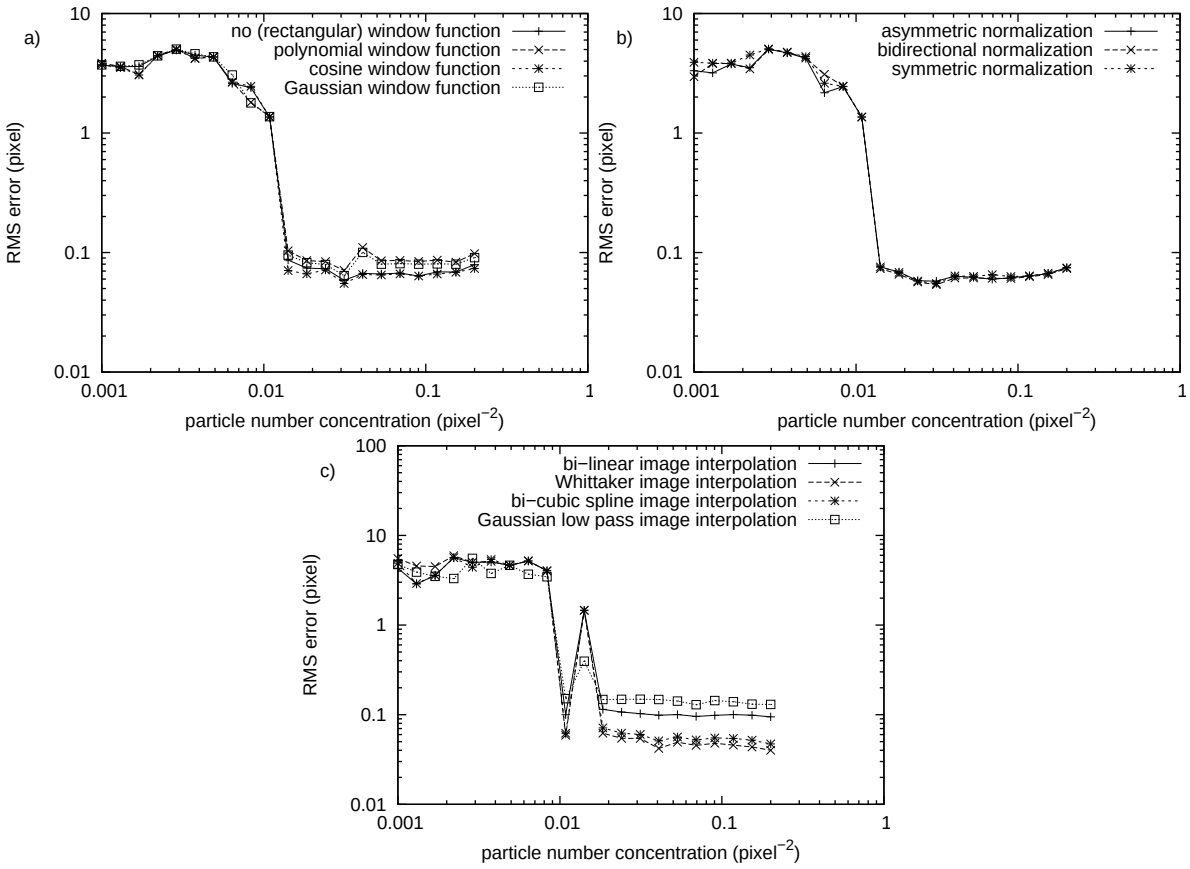

Figure 9: RMS deviation of the displacement estimate using a) the FFT with a window function b) the direct correlation with a normalization and c) the iterative interrogation area deformation with image interpolation as a function of the particle number concentration

images in the interrogation area and the increased probability of overlapping particle images and the resulting influence of the individual particle intensity variations compensate each other. Here again the iterative interrogation area shift and deformation with the Whittaker or bi-cubic spline image interpolation perform best, while the one-step estimators stay behind. The iterative interrogation area shift and deformation with the bi-linear interpolation or Gaussian low-pass interpolation are worse.

5.2 Iterative image deformation

To verify the performance of the iterative image deformation, the simulation procedure is slightly changed. The simulated displacement field is a two-dimensional sinusoidal wave as shown in Fig. 10. Therefore, the averaging influence of the interrogation area is evident. The estimation of the velocity values is done at grid points with a distance of 8 pixels in x and y direction.

Fig. 11 shows the RMS deviation as a function of the particle number concentration. In all cases a minimum particle number concentration is required to get reliable estimates without outliers. Above this lower concentration the iterative interrogation area deformation yields almost constant RMS deviations. The value depends on the interrogation area size and agrees with the expected deviation due to the spatial averaging over the interrogation area. Without an out-of-plane displacement (Fig. 11a) the iterative image deformation with interrogation area windowing nicely uses the available information. With an increasing particle number concentration the obtained RMS error decrease. For the large interrogation area of 32×32 pixel squared the obtained RMS error is even smaller than that of the interrogation area shift and deformation with an interrogation area of 16×16 pixel squared. This holds true also for simulated noise (Fig. 11b), whereas with a simulated out-of-plane displacement of $1/4$ of the light sheet width the results change significantly (Fig. 11c). Here the range of non-reliable estimates with outliers extends towards higher particle number concentrations. Furthermore, the interrogation area

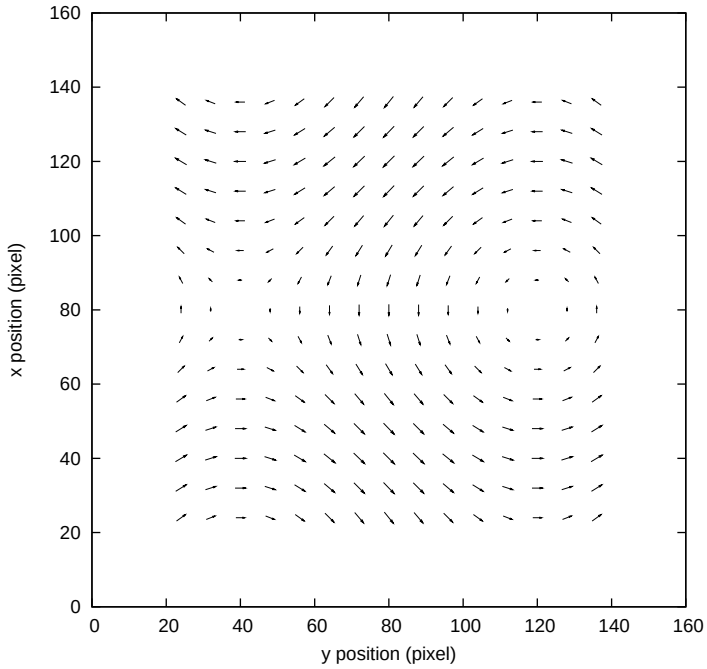

Figure 10: Simulated displcement field

shift and deformation with an interrogation area of 16×16 pixel squared does not reach the theoretical value of the averaging filter of corresponding size. However, the highest error has the image deformation. Here the higher resolution of the method makes the method more sensitive to the individual particle image intensity variations.

6 Conclusion

The effect of particle image intensities varying individually between the two consecutive images on the obtainable accuracy of a PIV system has been investigated. Such intensity variations occur in experiments due to the motion of the particles in the intensity profile of the light sheet or misalignments of the two light pulses.

For particle image diameters typically used in experiments, the error due to the individual particle intensity variations dominates over the error due to the under-sampling of the particle images. In the here investigated case of individually varying particle image intensities the application of windowing functions or the normalization of the correlation function to reduce the influence of truncated particle images at the interrogation area edges is found to be ineffectual. Furthermore, for the iterative methods, the bi-cubic spline or the Whittaker image interpolation give best, and among each other comparable results. The Gaussian low-pass filter image interpolation, which excellently performs without the intensity variations, has the highest RMS errors in the case of intensity variations.

The same holds true for the image deformation technique. The higher possible resolution on the one hand, on the other hand, yields a significantly higher sensitivity to the investigated effect of individually varying particle intensities. This effect, however, seriously limits the achievable accuracy.

In summary, the errors due to the variations of the particle image intensities may seriously limit the obtainable accuracy of PIV measurements and could explain the usually observed limit of about 0.1 pixel in experiments. This value is almost independent of the particle number concentration, but it decreases with increasing interrogation area size.

References

[1] T Utami, R F Blackwelder, and T Ueno. A cross-correlation technique for velocity field extraction from particulate visualization. *Exp. in Fluids*, 10:213–223, 1991.

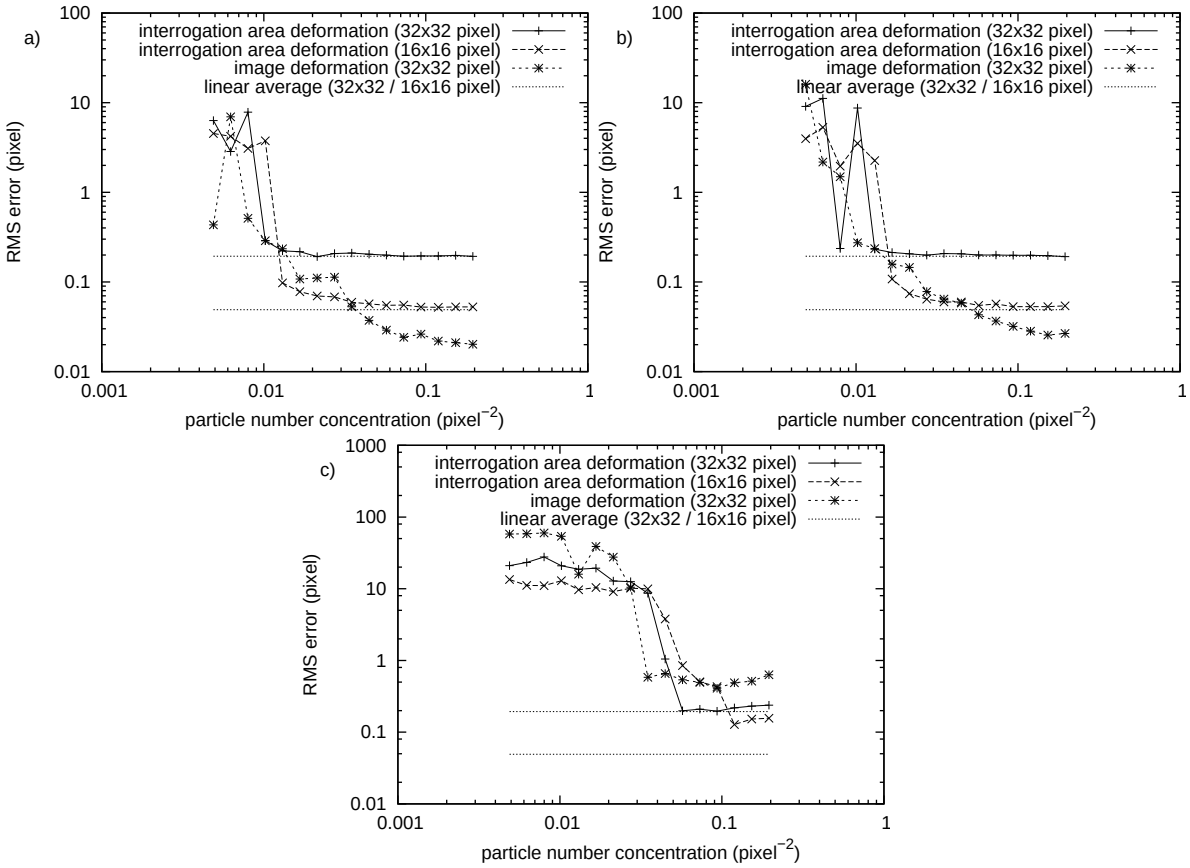

Figure 11: RMS deviation of the displacement estimate using the iterative image deformation with interrogation area windowing in comparison to the iterative interrogation area shift and deformation (top-hat windowing function): a) with only in-plane-motion, b) with only in-plane-motion and with noise and c) with out-of-plain motion ($^1/_4$ of the light sheet width) as a function of the particle number concentration

[2] C E Willert and M Gharib. Digital particle image velocimetry. *Exp. in Fluids*, 10:181–193, 1991.

[3] R D Keane and R J Adrian. Theory of cross-correlation analysis of PIV images. *Applied Scientific Research*, 49:191–215, 1992.

[4] J Westerweel. *Digital Particle Image Velocimetry: Theory and Application*. Delft University Press, Delft, The Netherlands, 1993.

[5] J S Morgan, D C Slater, J G Timothy, and E B Jenkins. Centroid position measurements and subpixel sensitivity variations with the MAMA detector. *Applied Optics*, 28(6):1178–1192, 1989.

[6] B F Alexander and K C Ng. Elimination of systematic error in sub-pixel accuracy centroid estimation. *Opt. Eng.*, 30:1320–1331, 1991.

[7] A K Prasad, R J Adrian, C C Landreth, and P W Offutt. Effect of resolution on the speed and accuracy of particle image velocimetry interrogation. *Exp. in Fluids*, 13:105–116, 1992.

[8] I Lourenco and A Krothapalli. On the accuracy of velocity and vorticity measurements with PIV. *Exp. in Fluids*, 18:421–428, 1995.

[9] A M Fincham and G R Spedding. Low cost, high resolution DPIV for measurement of turbulent fluid flow. *Exp. in Fluids*, 23:449–462, 1997.

[10] J Westerweel. Effect of sensor geometry on the performance of PIV. In *Proc. 9th Int. Symp. on Appl. of Laser Techn. to Fluid Mechanics*, Lisbon, Portugal, 1998.

[11] K T Christensen. The influence of peak-locking errors on turbulence statistics computed from PIV ensembles. *Exp. in Fluids*, 36:484–497, 2004.

[12] H Nobach, N Damaschke, and C Tropea. High-precision sub-pixel interpolation in PIV/PTV image processing. In *Proc. 12th Int. Symp. on Appl. of Laser Techn. to Fluid Mechanics*, Lisbon, Portugal, 2004. paper 24.1.

[13] T Roesgen. Optimal subpixel interpolation in particle image velocimetry. *Exp. in Fluids*, 35:252–256, 2003.

[14] J Chen and J Katz. Elimination of peak-locking error in PIV analysis using the correlation mapping method. *Meas. Sci. Technol.*, 16:1605–1618, 2005.

[15] J Nogueira, A Lecuona, and P A Rodriguez. Identification of a new source of peak locking, analysis and its removal in conventional and super-resolution PIV techniques. *Exp. in Fluids*, 30:309–316, 2001.

[16] J Nogueira, A Lecuona, and P A Rodriguez. Local field correction PIV: on the increase of accuracy of digital PIV systems. *Exp. in Fluids*, 27:107–116, 1999.

[17] L Gui, W Merzkirch, and R Fei. A digital mask technique for reducing the bias error of the correlation-based PIV interrogation algorithm. *Exp. in Fluids*, 29:30–35, 2000.

[18] Q Liao and E A Cowen. An efficient anti-aliasing spectral continuous window shifting technique for piv. *Exp. in Fluids*, 38:197–208, 2005.

[19] J Westerweel. Fundamentals of digital particle image velocimetry. *Meas. Sci. Technol.*, 8:1379–1392, 1997.

[20] H T Huang, H E Fiedler, and J J Wang. Limitation and improvement of PIV; part I: Limitation of conventional techniques due to deformation of particle image patterns. *Exp. in Fluids*, 15:263–273, 1993.

[21] H Huang, D Dabiri, and M Gharib. On error of digital particle image velocimetry. *Meas. Sci. Technol.*, 8:1427–1440, 1997.

[22] J Rohály, F Frigerio, and D P Hart. Reverse hierarchical piv processing. *Meas. Sci. Technol.*, 13:984–996, 2002.

[23] H T Huang, H E Fiedler, and J J Wang. Limitation and improvement of PIV; part II: Particle image distorsion, a novel technique. *Exp. in Fluids*, 15:263–273, 1993.

[24] B Lecordier. *Etude de l'interaction de la propagation d'une flamme premelangee avec le champ aerodynamique, par association de la tomographie Laser et de la Velocimetrie par Images de particules*. PhD thesis, l'Universite de Rouen, 1997.

[25] F Scarano. Iterative image deformation methods in PIV. *Meas. Sci. Technol.*, 13:R1–R19, 2002.

[26] O T Tokumaru and P E Dimotakis. Image correlation velocimetry. *Exp. in Fluids*, 19:1–15, 1995.

[27] K Jambunathan, X Y Ju, B N Dobbins, and S Ashforth-Frost. An improved cross correlation technique for particle image velocimetry. *Meas. Sci. Technol.*, 6:507–514, 1995.

[28] F Scarano. On the stability of iterative PIV image interrogation methods. In *Proc. 12th Int. Symp. on Appl. of Laser Techn. to Fluid Mechanics*, Lisbon, Portugal, 2004.

[29] T Astarita and G Cardone. Analysis of interpolation schemes for image deformation methods in piv. *Exp. in Fluids*, 38:233–243, 2005.

[30] J M Whittaker. The Fourier theory of the cardinal functions. *Proc. - R. Soc. Edinburgh Sect. A Math.*, 1:169–176, 1929.

[31] F Scarano and M L Riethmuller. Advances in iterative multigrid PIV image processing. *Exp. in Fluids*, 29:S51–S60, 2000.

[32] H Nobach, N Damaschke, and C Tropea. High-precision sub-pixel interpolation in particle image velocimetry image processing. *Experiments in Fluids*, 39:299–304, 2005.

[33] B Lecordier and M Trinité. Accuracy assessment of image interpolation schemes for PIV from real images of particle. In *Proc. 13th Int. Symp. on Appl. of Laser Techn. to Fluid Mechanics*, Lisbon, Portugal, 2006. paper 26.4.

[34] R D Keane and R J Adrian. Optimization of particle image velocimeters. part i: Double pulsed systems. *Meas. Sci. Technol.*, 1:1202–1215, 1990.

[35] R D Keane, R J Adrian, and Y Zhang. Super-resolution particle image velocimetry. *Meas. Sci. Technol.*, 6:754–768, 1995.

[36] J Westerweel. Theoretical analysis of the measurement precision in particle image velocimetry. *Exp. in Fluids*, 29:S3–S12, 2000.